



Ultrastructural visualization of the Mesenchymal-to-Epithelial Transition during reprogramming of human fibroblasts to induced pluripotent stem cells

Høffding, Miya Kudo; Hyttel, Poul

Published in:
Stem Cell Research

DOI:
[10.1016/j.scr.2014.11.003](https://doi.org/10.1016/j.scr.2014.11.003)

Publication date:
2015

Document version
Early version, also known as pre-print

Citation for published version (APA):
Høffding, M. K., & Hyttel, P. (2015). Ultrastructural visualization of the Mesenchymal-to-Epithelial Transition during reprogramming of human fibroblasts to induced pluripotent stem cells. *Stem Cell Research*, 64, 39-53. <https://doi.org/10.1016/j.scr.2014.11.003>



Available online at www.sciencedirect.com

ScienceDirect

www.elsevier.com/locate/scr



Ultrastructural visualization of the Mesenchymal-to-Epithelial Transition during reprogramming of human fibroblasts to induced pluripotent stem cells



M.K. Høffding*, P. Hyttel

Stem Cells and Embryology Group, Department of Veterinary Clinical and Animal Sciences, Faculty of Health and Medical Sciences, Copenhagen University, Groennegaardsvej 7, 1870 Frederiksberg C, Denmark

Received 26 June 2014; received in revised form 15 October 2014; accepted 22 November 2014

Abstract The Mesenchymal-to-Epithelial Transition (MET) has been recognized as a crucial step for successful reprogramming of fibroblasts to induced pluripotent stem cells (iPSCs). Thus, it has been demonstrated, that the efficiency of reprogramming can be enhanced by promoting an epithelial expression program in cells, with a concomitant repression of key mesenchymal genes. However, a detailed characterization of the epithelial transition associated with the acquisition of a pluripotent phenotype is still lacking to this date.

Here, we integrate a panel of morphological approaches with gene expression analyses to visualize the dynamics of episomal reprogramming of human fibroblasts to iPSCs. We provide the first ultrastructural analysis of human fibroblasts at various stages of episomal iPSC reprogramming, as well as the first real-time live cell visualization of a MET occurring during reprogramming. The results indicate that the MET manifests itself approximately 6–12 days after electroporation, in synchrony with the upregulation of early pluripotency markers, and resembles a reversal of the Epithelial-to-Mesenchymal Transition (EMT) which takes place during mammalian gastrulation.

© 2014 The Authors. Published by Elsevier B.V. This is an open access article under the CC BY-NC-ND license (<http://creativecommons.org/licenses/by-nc-nd/3.0/>).

Introduction

In 2006, Shinya Yamanaka's group made the groundbreaking discovery that somatic cells could be reprogrammed to induced pluripotent stem cells (iPSCs) by retroviral

overexpression of the four embryonic transcription factors OCT4, C-MYC, SOX2 and KLF4 (abbreviated OMSK) (Takahashi and Yamanaka, 2006). This paved the road for a new era of stem cell research involving the generation of patient-specific stem cells and disease models, and a vision

Abbreviations: iPSCs, induced pluripotent stem cells; ESCs, embryonic stem cells; MEFs, mouse embryonic fibroblasts; OMSK, OCT4 + C-MYC + SOX2 + KLF4; EMT, Epithelial-to-Mesenchymal Transition; MET, Mesenchymal-to-Epithelial Transition; NHDFs, Normal Human Dermal Fibroblasts; qPCR, quantitative PCR; GFP, green fluorescent protein.

* Corresponding author.

E-mail addresses: mkudo@sund.ku.dk (M.K. Høffding), poh@sund.ku.dk (P. Hyttel).

<http://dx.doi.org/10.1016/j.scr.2014.11.003>

1873-5061 © 2014 The Authors. Published by Elsevier B.V. This is an open access article under the CC BY-NC-ND license (<http://creativecommons.org/licenses/by-nc-nd/3.0/>).

of performing autologous transplantation for various degenerative diseases in the future. The fact that self-renewing pluripotent stem cells could be generated from almost any type of differentiated cell, provided researchers with an inexhaustible pool of pluripotent stem cells, and circumvented many of the ethical concerns associated with human embryonic stem cells (ESCs). Thus, iPSCs are increasingly applied as a complementary strategy to ESCs in stem cell research today.

Since Yamanaka's remarkable findings, much effort has been invested in revealing the pathways leading to reactivation of the endogenous pluripotency apparatus in differentiated cells, and in identifying factors which regulate this process. In 2010 it was reported that during the course of iPSC reprogramming, mouse embryonic fibroblasts (MEFs) transition from a mesenchymal phenotype into an epithelial phenotype, before reaching the pluripotent state (Li et al., 2010; Samavarchi-Tehrani et al., 2010). Transitions between epithelial and mesenchymal states are well known from embryonic development, for example during gastrulation, when epithelial cells from the pluripotent epithelial epiblast ingress through the primitive streak to form the mesodermal and endodermal lineages, and during neurulation when neural crest cells delaminate from the neural epithelium at the hinge point of the neural groove (Kalluri and Weinberg, 2009). Morphologically, these examples of so-called Epithelial-to-Mesenchymal Transitions (EMTs) are characterized by a switch from an epithelial columnar cell type with apical–basal polarity defined by the anchorage to neighboring cells via tight junctions, adherens junctions and desmosomes, towards a spindle-shaped and solitary cell type with migratory protrusions and invasive capacity (Ferrer-Vaquer et al., 2010). Crucially for this to occur, the Actin cytoskeleton must rearrange from a terminal web into stress fibers. At the molecular level, EMT involves a coordinated downregulation of epithelial markers such as E-cadherin, Zo-1 and Cytokeratin and upregulation of mesenchymal markers such as Vimentin, Snai1/2, ZEB1 and N-Cadherin (Zeisberg and Neilson, 2009). Mesenchymal-to-Epithelial Transition (MET) represents the reverse process of EMT and also occurs during embryonic development, for example when mesenchymal cells, which have ingressed through the anterior primitive streak, form the foregut endoderm epithelium (Ferrer-Vaquer et al., 2010).

The MET occurring during reprogramming appears to be an important step towards the full dedifferentiation of fibroblasts to iPSCs (Li et al., 2010; Samavarchi-Tehrani et al., 2010; Liao et al., 2011a; Subramanyam et al., 2011a; Shu and Pei, 2014). Li et al. showed that the transcription factors OMSK work in concert during reprogramming of MEFs to suppress EMT drivers and promote expression of epithelial markers. In addition, they demonstrated that blocking or reversing the MET during reprogramming resulted in significant reduction in the number of emerging pluripotent colonies (Li et al., 2010). Accordingly, the Wrana lab divided the reprogramming of MEFs into three phases termed Initiation, Maturation and Stabilization, based on gene expression profiling, and reported MET as a hallmark of the Initiation phase between days 0 and 5 post-transduction (Samavarchi-Tehrani et al., 2010). Following up on these findings, several groups have identified microRNAs (Lee et al., 2013; Wang et al., 2013; Liao et al., 2011b; Li et al.,

2011), genes (Chen et al., 2012; Takahashi et al., 2014; Sakurai et al., 2014) and epigenetic modifiers (Hu et al., 2014; Onder et al., 2012; Liang et al., 2012) which enhance reprogramming by promoting MET, either directly by stimulating the expression of epithelial proteins, or indirectly by inhibiting EMT inducing signals. Thus, extensive research on cell signaling and gene regulation points towards an important, and potentially causal, link between cell epithelialization and gain of pluripotent characteristics. However, surprisingly few iPSC studies have focused on characterizing the morphogenesis of solitary somatic cells turning into a pluripotent epithelium. In fact, to our knowledge there has been no ultrastructural report on the dynamics of iPSC reprogramming to date. How exactly do changes in gene expression during reprogramming correlate with changes in cell–cell organization, cytoskeletal architecture, and secretory pathway components? Can parallels be drawn to the pluripotent epithelium of the mammalian epiblast? In other words, does transcription factor reprogramming involve the same dynamic patterns of intercellular contact and communication as those seen during embryonic development? These are the questions we seek to elucidate in this study. To this end, we present an ultrastructural characterization of human fibroblasts undergoing reprogramming to iPSCs, and compare this to the ultrastructure of porcine gastrulation.

Materials and methods

Cell culture

Adult Normal Human Dermal Fibroblasts (NHDFs) were purchased from Lonza (Clonetics™ Human Fibroblast Cell Systems, CC-2511). Cells were seeded in the Corning T175 flasks (Sigma, CLS431079) coated with 0.1% gelatin (Sigma-Aldrich, G2500) and cultured in Dulbecco's modified Eagle's medium with 4500 mg/L glucose (DMEM-AQmedia™, Sigma-Aldrich, D0819) supplemented with 10% FBS (GIBCO, 10270-098) and 100 µg/mL penicillin/streptomycin (Sigma-Aldrich, P0781) at 37 °C in a humidified atmosphere of 5% CO₂ (fibroblast conditions). Medium was replaced every other day, and cells were enzymatically passaged with Trypsin–EDTA (Sigma-Aldrich, T3924) when reaching 90% confluence. iPSCs were kept in 6 well plates coated with ESC-qualified BD Matrigel™ (BD Biosciences, 354277) and cultured in mTeSR™1 (Stemcell Technologies, 05850) at 37 °C in a humidified atmosphere of 5% CO₂, 5% O₂ and 90% N₂ (stem cell conditions). Medium was replaced every other day, and colonies were manually passaged with an insulin needle (Myjector U-100 0.5 mL 27Gx1/2", Terumo, BS05M2713) every 5–7 days.

Episomal plasmids, electroporation and reprogramming

Episomal plasmids pCXLE-hUL, pCXLE-hSK and pCXLE-hOCT3/4-shp53-F were published by Okita et al. (2011) and modified from Niwa et al. (1991). All plasmids were purchased from Addgene (27080, 27078, 27077) and purified with the Purelink® HiPure Plasmid Maxiprep kit (Invitrogen, K2100-06). For each replicate, a total of 1 µg DNA (plasmids mixed 1:1:1) was electroporated into 100,000 NHDF P5-7 in suspension using the

Neon™ Transfection System (Invitrogen, MPK5000) with a protocol of 2 pulses at 1200 V and pulse width of 20 ms (efficiency of electroporation: 65–70%, $n = 3$). Electroporated cells were seeded in 6 well plates (10^5 cells/well) coated with 0.1% gelatin and maintained under fibroblast conditions until day 6 post-electroporation when they were transferred to stem cell conditions (80,000 cells/well). On days 20–24, iPSCs were manually picked.

Cells were collected for analyses on days 0, 6, 9, 12 and 18 of reprogramming as well as after passaging of iPSC colonies.

Vimentin promoter-GFP cell line

The human Vimentin promoter-EGFP construct is described in [Bindels et al. \(2006\)](#), [Gilles et al. \(1999\)](#) and [Gilles et al. \(2003\)](#) and was kindly provided by Dr. Christine Gilles, Laboratory of Developmental and Tumor Biology, Tour de Pathologie, B23, 4000 Liège, Belgium. NHDFs were electroporated with the Vimentin promoter-EGFP construct using the settings described in the [Episomal plasmids, electroporation and reprogramming](#) section followed by a 14 day selection with 500 $\mu\text{g}/\text{mL}$ G418. Then, fibroblasts were reprogrammed according to the [Episomal plasmids, electroporation and reprogramming](#) section, and used for real time non-invasive imaging as described in the [Real-time non-invasive imaging](#) section. Additionally, transfected fibroblasts were enriched by FACS after the G418 selection to ensure a starting population with a homogenous GFP signal. This population was reprogrammed according to the [Episomal plasmids, electroporation and reprogramming](#) section and used for immunocytochemistry.

RNA isolation and quantitative PCR (qPCR)

Cells were detached with trypsin–EDTA and RNA was isolated using the RNeasy Micro Plus kit (Qiagen, 74034). 1 μg of purified RNA was reverse transcribed into cDNA using the RevertAid First Strand cDNA Synthesis kit (Thermo Scientific, K1622). Comparative real-time qPCR was performed on a Roche Lightcycler using SYBR Green I Master Mix (Roche, 04887352001). All primers were previously published and verified by melting curve analysis and gel electrophoresis. Sequences and references are listed in Supplementary Table S2. Data analysis was performed according to the $\Delta\Delta\text{Ct}$ method using ACTB as endogenous control, and values from NHDFs at day 0 of reprogramming were used as a calibrator for relative quantification. The results are presented as mean \pm S.D. of three independent experiments.

Immunofluorescence

Cells were seeded on Thermo Fisher Scientific Lab-Tek chamber slides (Sigma-Aldrich, C6932) coated with 0.1% gelatin or BD Matrigel™. Cells were fixed in 4% formaldehyde in PBS for 10 min, washed with PBS and permeabilized with 1% Triton X-100 (Merck, 1086431000) for 15 min. Blocking was performed with 10% normal donkey serum (Millipore, S30) in 1% BSA/PBS (Sigma-Aldrich, A7906) for 30 min at room temperature followed by incubation with primary

antibodies in 1% BSA/PBS at 4 °C overnight. The next day, cells were washed with PBS, incubated with secondary antibodies for 1 h at room temperature and washed in PBS again before counterstaining with 1 $\mu\text{g}/\text{mL}$ Hoechst (Life Technologies, H3570) for 10 min at room temperature. Coverslips ($24 \times 50 \times 0.16$ mm, Hounisen, 0422.2450) were then mounted with fluorescent mounting medium (DAKO, S3023). Antibodies and concentrations are listed in Supplementary Table S3.

Images were obtained with a Leica TCS SP5 II inverted confocal laser-scanning microscope with a UV laser, an Argon laser and a HeNe laser, and a freely tunable AOBBS beam splitter. Acquisition was performed with a 40 \times objective (Leica PL FLUOTAR, OIL, NA = 1.00) at a pinhole size of 0.7 airy units. Pictures were post-processed using LAS AF Lite software and Adobe Photoshop CS4.0.

Transmission electron microscopy (TEM)

Cells were seeded on 13 mm Thermanox Plastic Coverslips (NUNC, 174950) coated with 0.1% gelatin or BD Matrigel™ and cultured as described in the [Cell culture](#) section. On the day of fixation, cells were washed twice in PBS and fixed in 3% glutaraldehyde (Merck, 1042390250) in 0.1 M Na-phosphate buffer for 1 h. Coverslips were cut into pieces of approximately 2 mm \times 5 mm and embedded in 4% LB-agar at 45 °C (Sigma-Aldrich, L2897). Specimens were then washed twice in 0.1 M Na-phosphate buffer, postfixed in 1% OsO₄ in 0.1 M Na-phosphate buffer for 1 h at room temperature followed by washing twice in 0.1 M Na-phosphate buffer and distilled water, respectively. Samples were dehydrated in a series of ascending ethanol concentrations (50% EtOH for 10 min, 70% EtOH for 10 min, 96% EtOH for 10 min, 99% EtOH for 3 \times 20 min) followed by washing with propylene oxide (Merck, 8070271000) for 2 \times 10 min. Samples were embedded in Epon (812 Resin, TAAB T031) using propylene oxide as an intermedium and polymerized for 24 h at 60 °C. Semi-thin sections of 2 μm were cut with glass knives (LKB Bromma 7800, Leica Microsystems) on an ultramicrotome (Reichert Ultracut S, Leica, Microsystems) and stained with 1% toluidine blue O (Millipore 1159300025). Ultra-thin sections (70 nm) were sectioned with a diamond knife (Jumdi, 2 mm) on an ultramicrotome (Reichert Ultracut UCT, Leica) and stained with 2% uranyl acetate (Polyscience, 21447) and lead citrate ([Reynold, 1963](#)). Sections were collected on 150 mesh copper grids (Gilder, G150-C3) coated with a parlodion/ amyl acetate film (EMS) and imaged with a Philips CM100 transmission electron microscope equipped with a Morada camera. Preparation of the porcine embryonic disc for transmission electron microscopy was described in [Hall et al. \(2010\)](#) and [Wolf et al. \(2011\)](#). For each time point, 2–5 replicates were processed.

Scanning electron microscopy (SEM)

Cells were cultured, fixed and dehydrated in EtOH as described in the [Immunofluorescence](#) section, with exception of the agar embedding step. Coverslips were cut into pieces of approximately 0.5 cm \times 0.5 cm and critical point dried (Electron Microscopy Sciences, EMS850) before

mounting on carbon conductive tabs on aluminium stubs and sputter coating with 5–30 nm gold/palladium (Quorum Technologies, SC7640). Micrographs were obtained with a FEI Quanta 200 Scanning electron microscope at an accelerating voltage of 3–10 kV and images were processed in Adobe Photoshop CS4.0. For each time point, 3 replicates were processed.

Real-time non-invasive imaging

Human Vimentin-promoter-EGFP fibroblasts undergoing reprogramming to iPSC were placed in a Nikon Biostation IM Version 2.21 on day 6 after electroporation. Phase contrast and FITC images were captured every 15 min over a 10 day interval (days 6–15 of reprogramming).

Results

Human fibroblasts form an epithelium within the first 12 days of episomal reprogramming

Reprogramming of fibroblasts to iPSCs involves profound changes in cell shape and behavior, ultimately resulting in the morphogenesis of solitary mesenchymal cells into colonies of tightly adhering epithelial cells. In order to unravel the dynamics of this process at the ultrastructural level, NHDFs were electroporated with non-integrating episomal plasmids encoding OCT4, SOX2, KLF4, L-MYC, LIN28 and a short hairpin targeting P53, and cultured under fibroblast conditions the first week of reprogramming. Then, cells were passaged to stem cell conditions and cultured for another 14–18 days before manual picking and clonal expansion (Fig. 1A). This culturing procedure was based on the protocol for episomal reprogramming published by Yamanaka and group in 2011 (Okita et al., 2011), and resulted in a reprogramming efficiency of approximately 0.2% ($n = 15$, see Table 1). In addition, we tried to culture transfected fibroblasts under stem cell conditions from day 1 post-electroporation, thus omitting the fibroblast culture period and the trypsinization step on day 6. However, under these stem cell conditions, no iPSC colonies emerged within 30 days ($n = 3$, results not shown).

SEM revealed that prior to reprogramming NHDFs were elongated and flattened with an average length of approximately 100 μm . The fibroblasts contained large nucleoli and a prominent perinuclear endoplasmic reticulum (ER), and they presented lamellipodia and filopodia characteristic of migratory cells (Fig. 1B, NHDF). At D6, subpopulations of smaller and more compact cells were found among the fibroblasts. These cells had fewer migratory protrusions and some of them showed a sporadic distribution of microvilli on their surface (Fig. 1B, D6). At D12, dense and round iPSC-like colonies were found nesting in the surrounding sheet of fibroblasts. Cells in these colonies varied greatly in size and surface structure, displaying diameters ranging from 5 to 30 μm and various degrees of microvilli density (Fig. 1B, D12). Finally, on D18, colonies had increased their diameter three to four-fold, and cells appeared more uniform in size than on day 12 (Fig. 1B, D18). Overall, the scanning electron microscopy indicated that NHDFs obtained epithelial characteristics during the first 12 days of episomal

reprogramming, after which colonies matured into a more homogenous population of epithelial cells.

The SEM observations were elaborated by TEM of cells at five different stages of reprogramming (Fig. 2). Cross sections of NHDFs at D0 confirmed that prior to reprogramming the fibroblasts displayed a smooth surface without microvilli and intercellular junctions (Fig. 2, D0B–C). The cytoplasm was dominated by intermediate filaments and a prominent rough ER (Fig. 2, D0E). This phenotype was retained up to D6, when horizontal sections revealed well developed Golgi stacks (Fig. 2, D6E). A few cells displayed a sparse and random distribution of microvilli on their surface (Fig. 2, D6B), indicating the potential initiation of a MET. At D9, some cells had assumed a more rounded shape with a higher nuclear: cytoplasmic ratio and fewer migratory protrusions (Fig. 2, D9A). In some cases, the plasma membranes of adjacent cells carried microvilli and were closely apposed, but no signs of intercellular junctions were found (Fig. 2, D9B–C). The cytoplasmic content primarily consisted of free polyribosomes and mitochondria, whereas organelles of the secretory pathway such as ER and Golgi complexes were no longer present (Fig. 2, D9E). At D12, some of the cells in iPSC-like colonies had acquired a columnar shape, and they were aligned side by side in a loosely arranged monolayered epithelium (Fig. 2, D12A). Mitoses were commonly observed at the apical face of colonies (Fig. 2, D12A). Some cells carried microvilli and were tethered to their neighbors by tight junctions, adherens junctions and gap junctions (Fig. 2, D12B–C). These cells rested on a basement membrane, under which a few solitary cells were sporadically distributed (Fig. 2, D12A). Other cells were in close apposition, but not yet in junctional contact with their neighbors, or with the basement membrane (Fig. 2, D12D). In general, the cells contained large nuclei with prominent nucleoli, and the cytoplasm was dominated by mitochondria, free polyribosomes and vacuoles (Fig. 2, D12D–E). Curiously, annular gap junctions were found in some cells on both D12 and D18 (Fig. 2, D12E). On D18, the colonies had matured into a well-structured sheet-like columnar epithelium with a continuous apical surface covered by microvilli and sealed by tight junctions, adherens junctions and desmosomes (Fig. 2, D18A–C). Besides free polyribosomes, the cells contained primarily mitochondria and lysosomes (Fig. 2, D18D–E).

In summary, the ultrastructural characterization of episomal reprogramming demonstrates that human fibroblasts retain most of their mesenchymal characteristics up until D6 of reprogramming, and that they appear to initiate an epithelial transition between days 6 and 12. Days 12 to 18 presumably involve maturation of the epithelial phenotype.

The MET associated with iPSC reprogramming shares ultrastructural similarities with the EMT occurring during mammalian gastrulation

Since human iPSC cells are classified as “primed” or “epiblast-like”, we were curious to see if we could spot any resemblance between the development of iPSCs *in vitro*, and the development of the mammalian epiblast *in vivo*. In other words, we were interested in analyzing whether the MET occurring during iPSC reprogramming would resemble a rewinding of the morphological changes associated with EMT

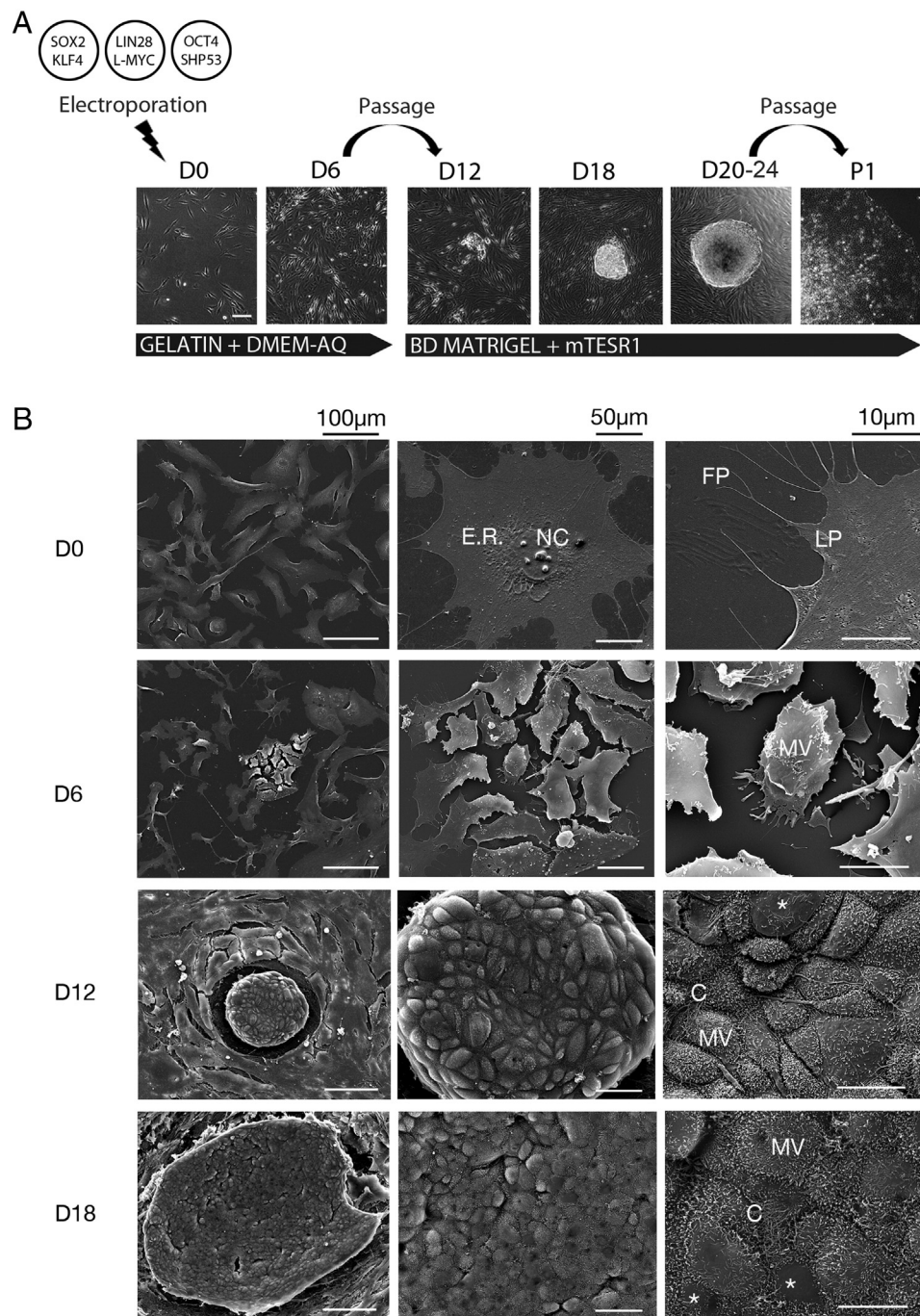


Figure 1 Human fibroblasts form iPSC colonies around day 12 of episomal reprogramming. (A) On day 0 (D0) NHDFs were electroporated with episomal plasmids and cultured on 0.1% gelatin in fibroblast medium (DMEM-AQ). After six days (D6), cells were trypsinized and transferred to stem cell culture conditions consisting of BD Matrigel and mTeSR1. Approximately two weeks later (D20–24), colonies were manually picked and expanded. Scale bar: 100 µm. (B) NHDFs were fixed with 6 day intervals during episomal reprogramming and processed for scanning electron microscopy. NC: nucleoli, ER: endoplasmatic reticulum, LP: lamellipodia, FP: filopodia, MV: microvilli, C: cilia, *: Cells with few or no microvilli. N = 3 for each time point. Scale bars in left column: 100 µm, scale bars in middle column: 25 µm, and scale bars in right column: 10 µm.

at gastrulation. Hence, we analyzed different stages of the porcine gastrulation by TEM, aiming at identifying parallels to the ultrastructural features presented for iPSC reprogramming above. In longitudinal sections placed through the primitive streak of porcine embryos at day 12, the epiblast was characterized by a pseudostratified columnar epithelium with

microvilli covering the apical surface, and cells linked by prominent tight junctions, intermediate junctions and desmosomes. On the basal side, epiblast cells were resting on a basement membrane beneath which loose mesendodermal progenitor cells were located. Underneath these, the hypoblast was found (Fig. 2, lower panel). This stage of the porcine

Table 1 Quantification of iPSC-like colonies undergoing MET during reprogramming.

NHDFs were fixed on D12 and D18 of reprogramming and processed for double immunofluorescent labeling of E-cadherin with Actin, Beta-catenin, Occludin, Vimentin, SSEA3 and TRA-1-60. For each combination of antibodies, the number of single or double positive colonies was counted on D12 and D18 and given as a percentage of the total number of colonies. N denotes the number of reprogrammings which the countings are based on. Representative images of the stainings are presented in Supplementary Fig. S1.

Marker combination	D12			D18		
	%	Colonies	N	%	Colonies	N
E-cadherin +/cortical Actin	100	43	3	100	57	3
E-cadherin +/cytoplasmic Actin	0			0		
E-cadherin –/cortical Actin	0			0		
E-cadherin +/cortical Beta-catenin	98	66	3	100	78	3
E-cadherin +/cytoplasmic Beta-catenin	0			0		
E-cadherin –/cortical Beta-catenin	1			0		
E-cadherin +/Occludin +	100	16	1	98	55	3
E-cadherin +/Occludin –	0			2		
E-cadherin –/Occludin +	0			0		
E-cadherin +/Vimentin +	0	14	1	0	30	1
E-cadherin +/Vimentin –	100			100		
E-cadherin –/Vimentin –	0			0		
E-cadherin +/TRA-1-60 +	86	22	2	71	35	2
E-cadherin +/TRA-1-60 –	14			26		
E-cadherin –/TRA-1-60 +	0			3		
E-cadherin +/SSEA3 +	(63)	24	2	86	43	3
E-cadherin +/SSEA3 –	37			14		
E-cadherin –/SSEA3 +	0			0		
Colony size	89 ± 37 μm	111	6	180 ± 105 μm	136	6

Average number of colonies on D18 per 10⁴ fibroblasts: 21.85 ± 6.77 (n = 15).

Reprogramming efficiency based on number of colonies per 10⁴ fibroblasts: 0.21%.

For each double immunofluorescent labeling, the most prevalent marker combination is emphasized in bold.

gastrulation roughly corresponds to the early trilaminar period of the human embryo (at the end of the second week) (Gasser, 1975). As epithelial cells from the porcine epiblast ingress through the primitive streak and breach the basement membrane to become mesendodermal progenitors, they transform from a columnar, polarized and tightly adhering phenotype, like that of mature iPSCs, into dissociated and solitary cells with migratory protrusions, comparable to cells at D6–9 of reprogramming. Thus, the ultrastructural changes associated with MET during reprogramming resemble a rewinding of the changes seen at EMT during gastrulation.

Episomal reprogramming of human fibroblasts can be divided into phases

To correlate the morphological observations with expression patterns of MET and pluripotency markers, immunocytochemistry and qPCR were performed on cells with six day intervals during reprogramming (Fig. 3). Table S1 provides an overview of the different markers, whose expression was analyzed.

Phalloidin staining of F-Actin revealed that cytoskeletal rearrangements could be detected as early as D6, when Actin changed distribution from stress fibers to a more cortical localization in a subpopulation of smaller cells. At D12, Actin was lining the plasma membrane of iPSC-like cells and had completely disappeared from the cytoplasm, giving the colonies a cobblestone-like appearance, which was preserved on D18 (Fig. 3A). The subcellular distribution of Beta-catenin

mimicked that of Actin, transitioning from the cytoplasm towards the plasma membrane during reprogramming, presumably in order to form adherens junctions between cells of developing iPSC colonies (Fig. 3A). Staining for the epithelial marker E-cadherin confirmed the establishment of adherens junctions at D12, whereas a weak Occludin signal indicated the initial formation of tight junctions around this time point (Fig. 3A). Onset of epithelial marker expression occurred simultaneously with expression of the pluripotency marker Nanog, and synchronized with a dramatic downregulation of the mesenchymal marker, Vimentin (Fig. 3A). Thus, immunocytochemistry confirmed an Initiation phase between D0 and D12, where cells 1) decreased in size and rearranged their Actin cytoskeleton (D0–D6); 2) lost their mesenchymal characteristics and initiated the formation of epithelial junctions (D6–12), 3) activated their endogenous pluripotency apparatus (D6–12); followed by a Maturation phase from D12 and onwards during which colonies became fully epithelial and increased in size.

In order to verify a correlation between the onset of an epithelial expression program and the acquisition of pluripotent characteristics, quantification of colony numbers was performed using multiple combinations of antibodies on reprogramming cells on D12 and D18 post-electroporation (Table 1 and supplementary Fig. S1). All E-cadherin positive colonies displayed a cobble-stone-like web of Actin on both D12 and D18 (100% of 43 and 57 colonies, respectively) as was the case for Beta-catenin (98% and 100% of 66 and 78 colonies, respectively), thus confirming the emergence of adherens junctions on D12. Expression of E-cadherin also

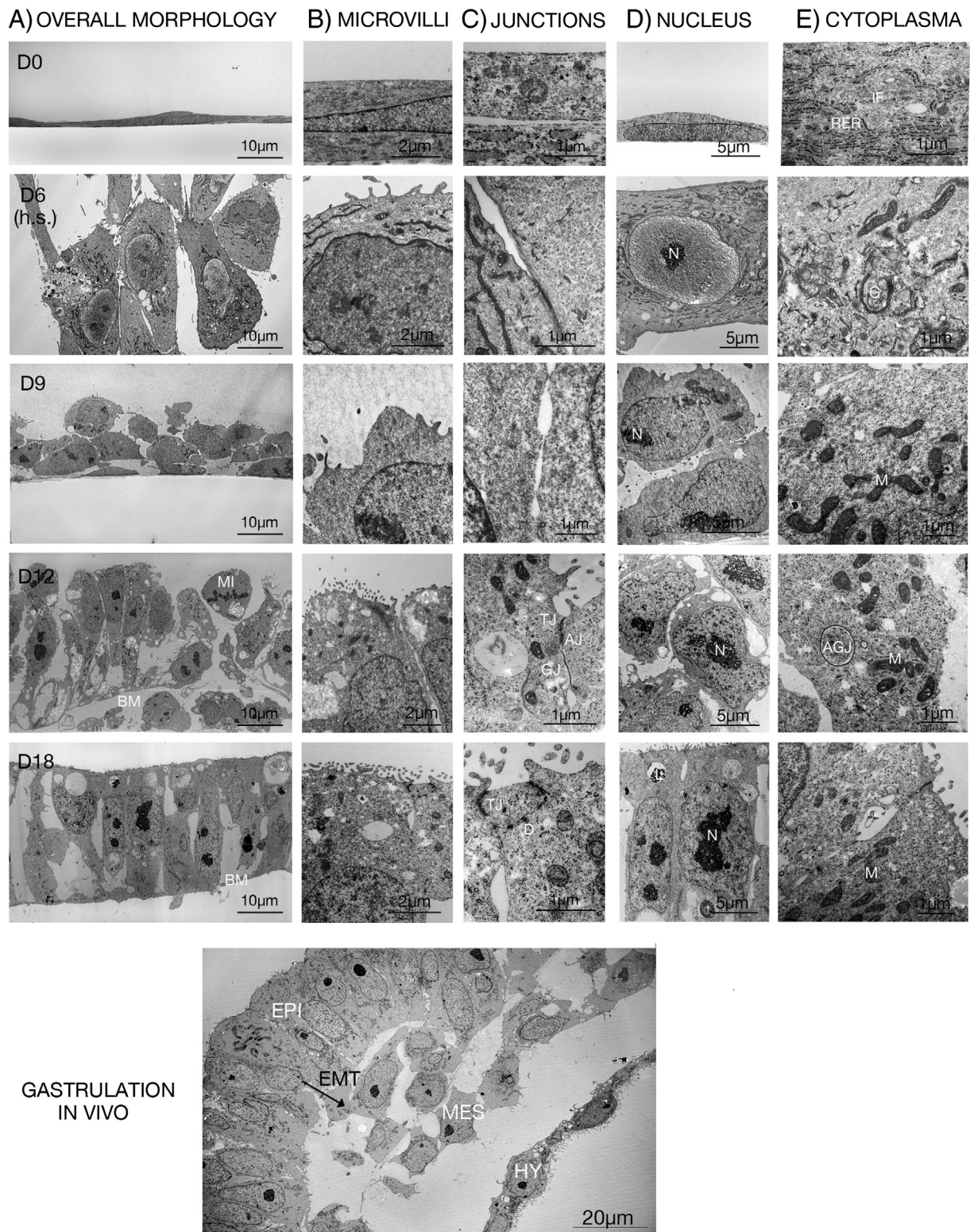
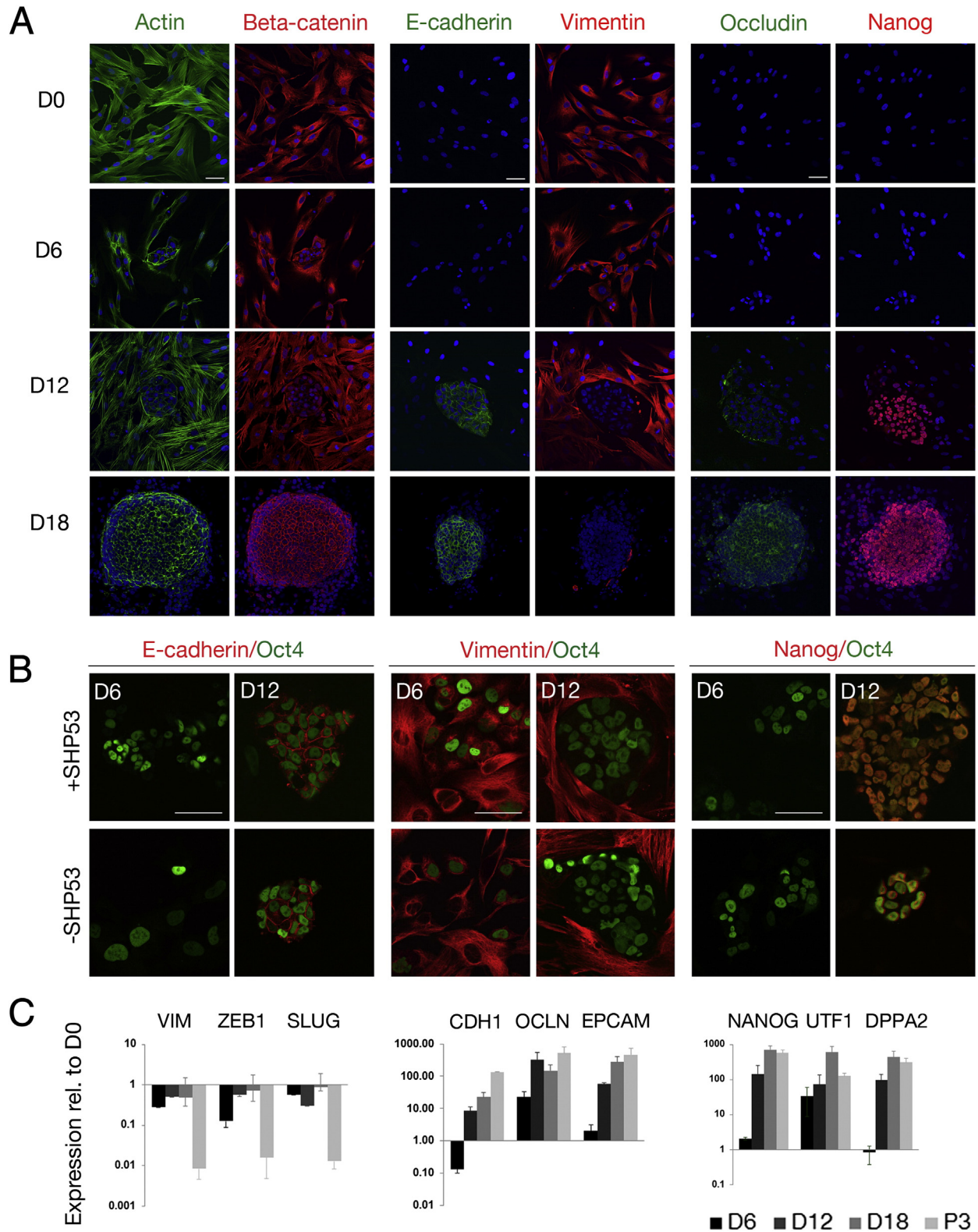


Figure 2 Human iPSCs acquire an epiblast-like morphology between days 12 and 18 of episomal reprogramming. NHDFs were fixed on days 0, 6, 9, 12 and 18 during reprogramming and processed for transmission electron microscopy. Images from D6 are based on horizontal sections (h.s.) All other images are from transverse sections. The porcine embryo was fixed around days 12–13 of gestation and sectioned vertically through the primitive streak. RER: rough endoplasmatic reticulum, IF: intermediate filaments, N: nucleolus, G: golgi, M: mitochondria, MI: mitosis, BM: basement membrane, TJ: tight junction, AJ: adherens junction, GJ: gap junction, AGJ: annular gap junction, D: desmosome, L: lysosome, EPI: epiblast, EMT: Epithelial–Mesenchymal Transition, MES: mesendoderm, HY: hypoblast. N = 2–5 for each time point.

positively correlated with expression of the tight junction marker Occludin on both D12 and D18 (100% and 98% of 16 and 55 colonies, respectively). There was a negative correlation between expression of E-cadherin and Vimentin in iPSC-like colonies on both D12 and D18 (100% of 14 colonies on D12, 100% of 38 colonies on D18) with all

E-cadherin positive colonies showing the absence of Vimentin. Overall, this confirms that the upregulation of epithelial markers during reprogramming was coordinated with the downregulation of mesenchymal markers within the same colonies. The majority of E-cadherin positive colonies were also positive for the pluripotency marker TRA-1-60 on



D12 and D18, signaling a positive correlation between the acquisition of epithelial and pluripotent characteristics (86% of 22 colonies on D12, 71% of 35 colonies on D18). However, only 63% of the E-cadherin positive colonies expressed the pluripotency marker SSEA3 on D12, and the expression was weak and heterogeneous in contrast to D18, when 86% of 43 E-cadherin positive colonies were clearly SSEA3 positive. This indicates that SSEA3 may be upregulated later than E-cadherin. Overall, the results suggest that the expression of epithelial markers and pluripotency markers occurs in an orchestrated fashion within the forming iPSC colonies between D12 and D18 of reprogramming.

It has been reported that knockdown of the tumor suppressor gene P53 can enhance reprogramming of MEFs to iPSC by accelerating MET (Brosh et al., 2013). In order to investigate whether the short hairpin targeting P53 in our reprogramming cocktail was altering the dynamics of MET we performed immunostainings of human fibroblasts undergoing reprogramming in the presence or absence of the hairpin. As shown in Fig. 3B, the coordinated expression of E-cadherin and Nanog with repression of Vimentin in transfected cells took place between D6 and D12, irrespective of P53 status (Hoechst overlays are displayed in Fig. S2). However, as was recently published by our group (Rasmussen et al., 2014), colonies were generally larger and more numerous when P53 was inhibited (Fig. 3B).

On the transcriptional level, the relative expression of mesenchymal markers VIM, ZEB1 and SLUG appeared constant or slightly downregulated throughout the first 18 days of reprogramming (Fig. 3C), in contrast to the dramatic reduction of all three markers in iPSC colonies at passage 3. This probably reflects the large number of non-reprogrammed fibroblasts in the samples from all time points prior to passage on day 20 (Fig. 1A). On the other hand, transcription of the epithelial markers CDH1, OCLN and EPCAM was dramatically increased from D12 and onwards, supporting the hypothesis that the MET initiates before D12 of reprogramming (Fig. 3C). Surprisingly, the transcription of CDH1 was downregulated between D0 and D6, thus challenging the assumption that fibroblasts are most mesenchymal-like at day 0 of reprogramming. However, expression of the tight junction gene OCLN was upregulated in this period, suggesting that on D6, mesenchymal cells were starting to tune in on an epithelial transition already at this early time point. The relative expression of early pluripotency markers Nanog, UTF1 and DPPA2 was increased to 100 fold at D12 of reprogramming,

and remained at a stable, high level during the remaining reprogramming period (Fig. 3C). Overall, the qPCR data indicated that the transcriptional activation of a MET program initiated between D0 and D12, and synchronized with onset of endogenous pluripotency.

Beta-catenin displays a dynamic subcellular distribution in cells undergoing reprogramming

As previously mentioned, Beta-catenin appeared to follow the distribution of Actin during reprogramming, transitioning from the cytoplasm of fibroblasts towards the plasma membranes of iPSCs. However, when looking closer at Beta-catenin localization in transfected cells co-immunostained for Oct4, we realized that on D6, Beta-catenin could be found in three different compartments in different cells (Fig. 4). In a minority of Oct4 positive cells, Beta-catenin was localized to the cytoplasm as on D0 of reprogramming (Fig. 4, D6A), whereas in the majority of transfected cells, there was a strong nuclear Beta-catenin signal on D6 (Fig. 4, D6B). Some cells with nuclear Beta-catenin signal also displayed a cortical distribution of Beta-catenin (Fig. 4, D6C), as shown on D12 and D18 (Fig. 3A). The cytoplasmic Beta-catenin signal was observed only in solitary and stellate fibroblast-like cells with prominent stress fibers, in contrast to the nuclear signal, which was associated with cells that had decreased in size and retracted their migratory protrusions. Cells displaying both nuclear and plasma membrane-associated localization of Beta-catenin on D6 were tightly associated with each other in small clusters, and they looked like daughter cells at the earliest stage of colony formation. These preliminary data may indicate that during reprogramming, Beta-catenin translocates from the cytoplasm into the nucleus before finally attending to the formation of adherens junctions at the plasma membranes of early iPSCs.

Live-cell imaging supports a MET between days 6 and 12 of reprogramming

Live cell imaging was performed to visualize the MET real-time during iPSC reprogramming. For this purpose, human fibroblasts containing a Vimentin promoter-GFP construct were electroporated with episomal plasmids, and their growth and behavior were monitored from D6 to D15 post-electroporation (Supplementary movie S1). Fig. 5A depicts a series of 24 hour interval snapshots of a

Figure 3 The MET is synchronized with the acquisition of pluripotent traits and occurs regardless of P53 status. (A) NHDFs were fixed with 6 day intervals during reprogramming and processed for double immunofluorescent labeling of: Beta-catenin/Actin to visualize changes in cytoskeletal arrangement; Vimentin/E-cadherin to visualize MET, and Occludin/Nanog to visualize a coordinated upregulation of epithelial and pluripotency markers. All images were acquired at the same magnification and are presented as overlays with Hoechst nuclear staining (blue). Scale bars: 50 μ m. (B) NHDFs were fixed on days 6 and 12 of reprogramming with or without a short hairpin targeting P53, and processed for double immunofluorescent labeling of Oct4 with E-cadherin, Vimentin, Nanog or SSEA4. All images were acquired at the same magnification and are presented as overlays. Scale bar: 50 μ m. (C) Cells from three independent experiments were processed for qPCR with 6 day interval during reprogramming, and after three passages (P3). Samples were measured in triplicate, and the mean values + standard deviations are shown for each of the indicated genes. All values are relative to day 0 and normalized to ACTB. Please note that the graphs have different log scales. *: $P > 0.05$, **: $P < 0.01$, ***: $P < 0.001$, ****: $P < 0.0001$.

reprogramming event, in which GFP-positive fibroblasts (encircled in red) give rise to a GFP-negative iPSC colony. The recording shows how two GFP positive cells cluster together and migrate as one compact unit at D6, after which the cells settle down and start dividing. Between D6 and D12, the cells in the cluster vary in size and shape, and they seem to divide and move around each other while remaining closely associated. On D11, the GFP signal in the colony begins to fade, and after 24 h it is barely detectable, supporting previous indications of Vimentin expression ceasing around D12 of reprogramming, when epithelial and pluripotent features initially develop. From D12 onwards, the cells and their offspring remain GFP-negative, and as they develop into a colony, they become more uniform in size. Please note that the GFP signal of fibroblasts at D6 varied among cells, as the transfected cell population was not clonal. Therefore, rather than identifying GFP negative cells as an evidence of MET, we were tracking only cells that were initially GFP positive. Fig. 5B displays immunostainings of the colony after 9 passages to verify the pluripotent state of the tracked cells. Fig. 5C displays Vimentin promoter-GFP fibroblasts which were FACS sorted prior to reprogramming to ensure that the starting population displayed a

homogenous, strong GFP signal. Reprogramming of this cell line was less efficient but nevertheless produced GFP negative colonies which were positive for Nanog, TRA-1-60 and E-cadherin on D12, and which could be passaged to >P7, thus confirming MET as a gateway for fibroblasts on the road to pluripotency.

In summary, we found that our reprogramming process from D0 to D18 involves a sequence of events which can be divided into an Initiation phase (D0–12) and a Maturation phase (D12–18) according to the nomenclature suggested by Samavarchi-Tehrani et al. (2010) (Fig. 6). During the first six days of the Initiation phase, cells are predominantly mesenchymal, but decrease in size and start to rearrange their Actin cytoskeleton. In this period, transcription of some epithelial and pluripotency markers appears to initiate, but on the translational and morphological level, these markers are not yet apparent. Between days 6 and 12 of the Initiation phase, cells replace their mesenchymal characteristics with epithelial and pluripotent features, in a process bearing inverse resemblance to the dynamics of the EMT occurring during mammalian gastrulation in vivo. The Maturation phase between days 12 and 18 involves expansion of the newly acquired epithelial and pluripotent phenotype.

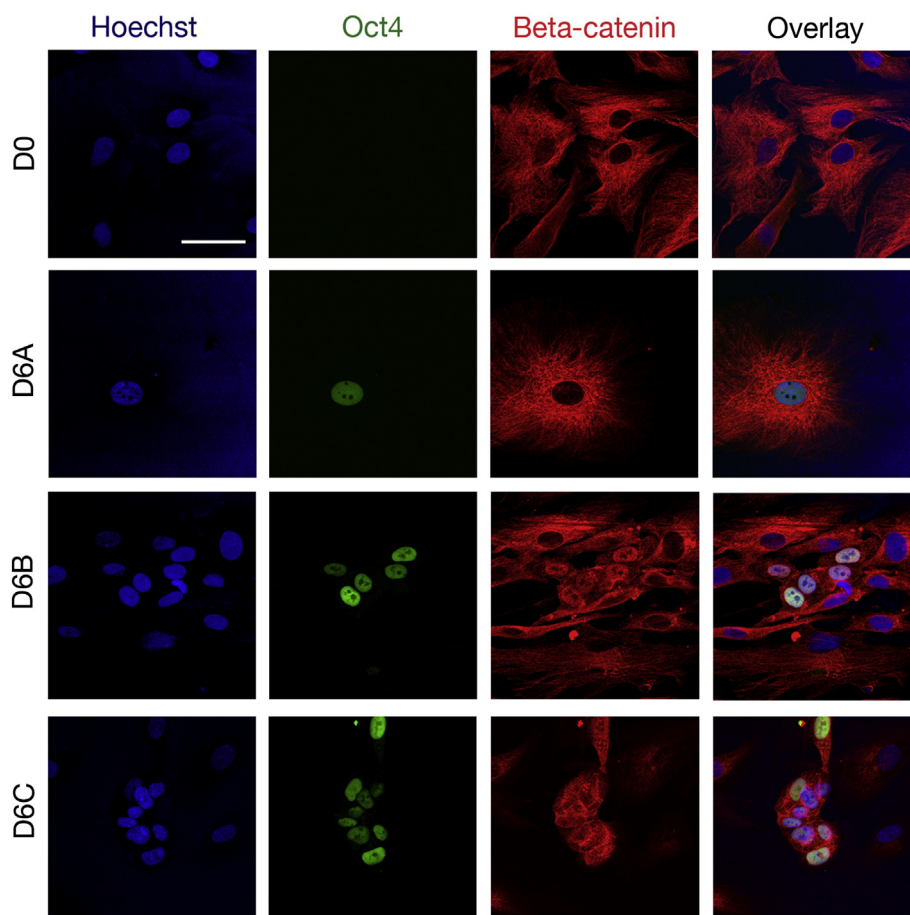


Figure 4 Beta-catenin translocates between cytoplasm, nucleus and plasma membrane during reprogramming. NHDFs were fixed with 6 day intervals during reprogramming and processed for double immunofluorescent labeling of Beta-catenin and Oct4 to visualize the localization of Beta-catenin in transfected cells. Here, three different cell phenotypes from day 6 are shown (D6A, D6B, D6C). All images were acquired at the same magnification. Scale bar: 50 μ m.

Discussion

The study of human embryonic development is challenged by ethical concerns associated with the use of in vitro fertilized donor material, or abortions, and by the limited access to such sample material. Consequently, the ultrastructural information about human epiblasts at the post-implantation stage is primarily based on findings from other species such as other primates, pigs and rodents (reviewed in (Pera and Trounson,

2004)). Here, we analyzed porcine gastrulation by TEM in order to decipher whether the MET occurring on the road to induced pluripotency mimics a reversal of the EMT which takes place during gastrulation in vivo. We were able to demonstrate that the artificial rewinding of differentiated human cells to induced pluripotency results in a cellular phenotype which resembles the human epiblast 7–12 days post-fertilization (Gasser, 1975; Hertig and Rock, 1945, 1949a, 1949b, 1949b). In this regard, one may speculate that the apical-to-basal

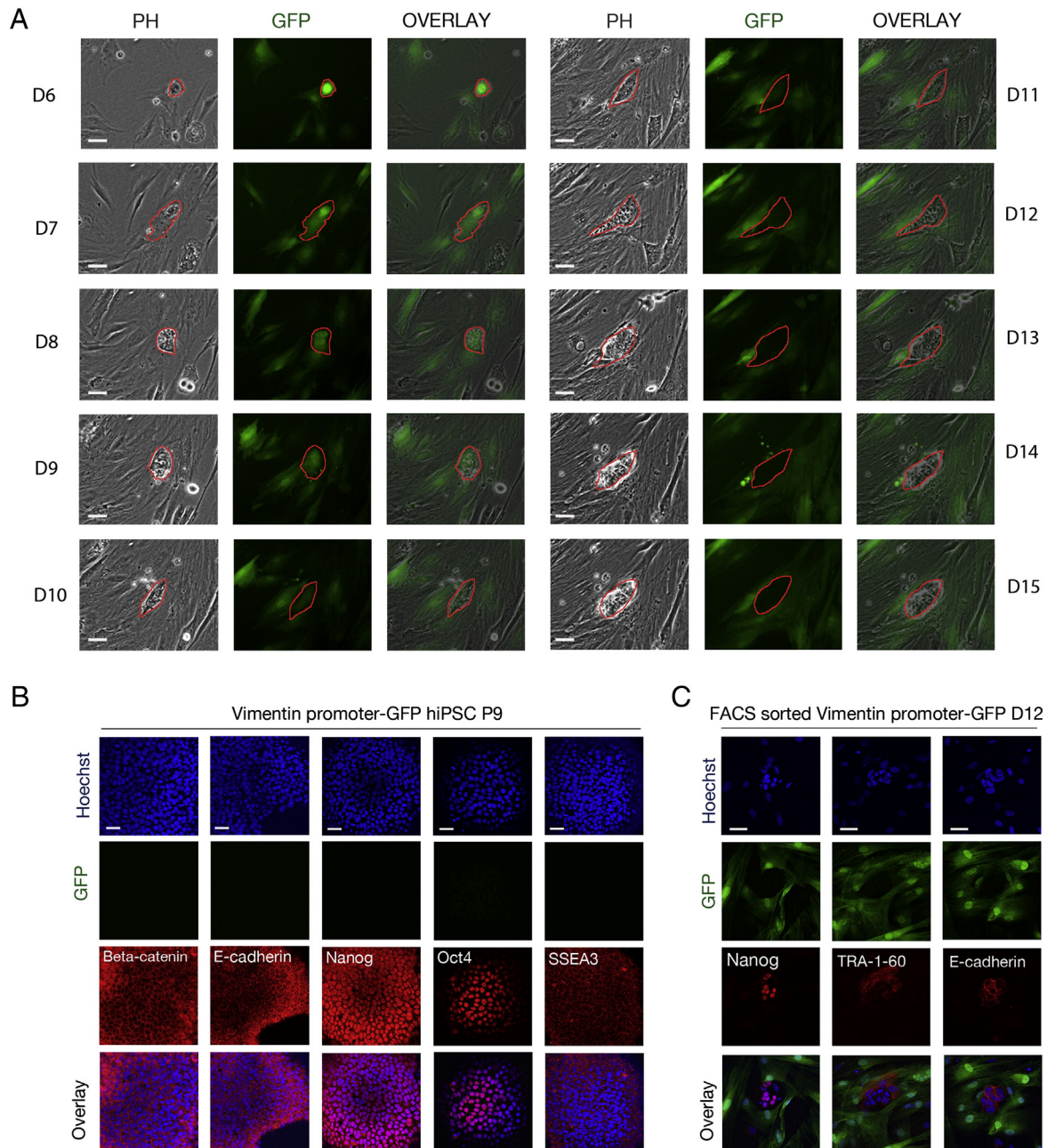


Figure 5 Live cell imaging confirms a MET around day 12 of reprogramming. (A) NHDFs carrying a Vimentin promoter-GFP reporter construct were monitored in a Biostation between days 6 and 15 of reprogramming. Phase contrast, epifluorescence and merged images are presented from left to right with 24 hour interval. The red ring marks tracking of cells which produce a Vimentin-negative colony. All images were acquired at the same magnification. Scale bars: 50 μ m. (B) The tracked colony was passaged and expressed cortical Beta-catenin and E-cadherin as well as the pluripotency markers Nanog, Oct4 and SSEA3 at P9. All images were acquired at the same magnification. Scale bar: 50 μ m. (C) FACS enriched Vimentin promoter-GFP NHDFs were fixed on D12 post-electroporation and labeled with Nanog, TRA-1-60 and E-cadherin to verify that MET occurs around D12 in reprogramming fibroblasts. Scale bars: 50 μ m.

migration of gastrulating epiblast cells during EMT is recapitulated in reverse order in iPSC colonies around day 12, when sporadically distributed mesenchymal-like cells underlying the early forming iPSC epithelium appear to move in the basal-apical direction up through the discontinuous basement membrane to become integrated as epithelial cells into the forming colony (Fig. 2, D12). The hypothesis that fibroblasts dedifferentiate to iPSC in a process which bears resemblance to a reverse gastrulation was recently supported by a publication from the Yamanaka group (Takahashi et al., 2014). They showed that TRA-1-60 positive human cells undergoing

reprogramming to iPSC had a transient gene expression profile reminiscent of primitive streak mesendoderm, and that overexpression of the transcription factor forkhead box H1 (FOXH1), which is crucial for the specification of the primitive streak, enhanced MET and the formation of iPSC (Takahashi et al., 2014). It would be interesting to visualize the morphogenesis of reprogramming cells which display this transient mesendodermal gene expression, in order to establish whether they resemble mesendodermal progenitors in the primitive streak on the morphological level. In present study, we were primarily analyzing cells in earlier stages of reprogramming

REPROGRAMMING OF HUMAN FIBROBLASTS TO IPSC

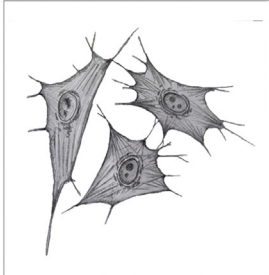
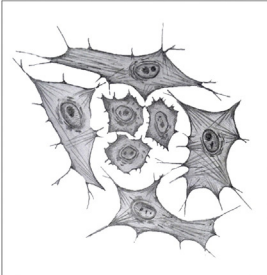
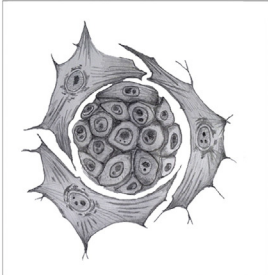

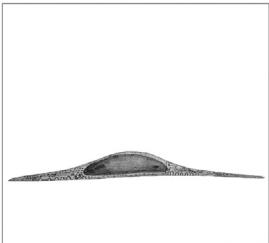
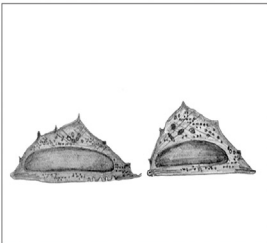

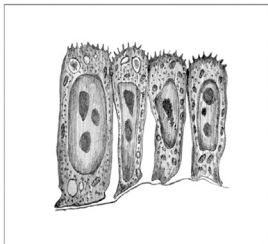
	DAY 0	DAY 6	DAY 12	DAY 18
TOP VIEW				
TRANSVERSE VIEW				
CELL CHARACTERISTICS	Cell size: 100µm Migratory protrusions Actin stress fibers Beta-catenin cytoplasm E.R., vesicles, Golgi, mitochondria, intermediate filaments VIM, ZEB1, SLUG	Cell size: 20-50µm (Microvilli) Cortical actin Beta-catenin cytoplasm/nuclear/plasma membrane E.R., vesicles, Golgi, mitochondria, intermediate filaments VIM, ZEB1, SLUG UTF1, OCLN	Cell size: 5-30µm Microvilli TJ, AJ, GJ, BM Actin terminal web Beta-catenin plasma membrane Free ribosomes, mitochondria, large vacuoles (ZEB1, SLUG) UTF1, OCLN, CDH1, EPCAM, NANOG, DPPA2	Cell size: 5-15µm Microvilli TJ, AJ, GJ, BM Actin terminal web Beta-catenin plasma membrane Free ribosomes, mitochondria, lysosomes (ZEB1, SLUG) UTF1, OCLN, CDH1, EPCAM, NANOG, DPPA2
	INITIATION		MATURATION	

Figure 6 Overview of morphological changes and gene expression dynamics during episomal reprogramming of human fibroblasts to iPSC. Abbreviations: TJ: tight junctions, AJ: adherens junctions, GJ: gap junctions, BM: basement membrane, E.R.: endoplasmic reticulum.

between D0 and D12, when no pluripotency markers were yet expressed, hence we cannot exclude the possibility that our ultrastructural characterizations were performed on partially reprogrammed cells. The correlation between acquisition of epithelial and pluripotent characteristics shown in Table 1 suggests that the epithelial iPSC-like colonies presented in Fig. 2 (D12, D18) were indeed destined to become true iPSCs. However, in order to fully confirm this, correlative light and electron microscopical analyses of TRA-1-60 positive cells undergoing reprogramming from D12 and throughout the maturation period would be needed.

Gene expression studies of partially or fully reprogrammed MEFs have led several groups to define distinct stages of reprogramming, as elegantly reviewed by David and Polo (2014). Generally, three phases are proposed; the first one being defined by MET, increased proliferation and cytoskeletal rearrangements (Li et al., 2010; Samavarchi-Tehrani et al., 2010; Sakurai et al., 2014; Mikkelsen et al., 2008; Sridharan et al., 2009; Stadtfeld et al., 2008; Polo et al., 2012; Hansson et al., 2012), the second comprising an intermediate or partial stage of reprogramming during which early pluripotency markers are upregulated (SSEA1 in mouse, TRA-1-60 in human, followed by Nanog and Oct4) (Sridharan et al., 2009; Stadtfeld et al., 2008; Polo et al., 2012; Hansson et al., 2012; Brambrink et al., 2008; Tanabe et al., 2013), and finally the third phase when passaged pluripotent colonies exhibit transgene independence, X-reactivation and telomere elongation (Mikkelsen et al., 2008; Sridharan et al., 2009; Stadtfeld et al., 2008; Brambrink et al., 2008). As previously mentioned, these three phases were named Initiation, Maturation and Stabilization by J. Wrana and group in 2010 (Samavarchi-Tehrani et al., 2010).

All of these studies categorize MET as an initial event during reprogramming which is followed by upregulation of the pluripotency machinery later in the process. Here we observed that in the time course of reprogramming human fibroblasts to iPSCs, the MET was preceded by a six day period (D0–6), during which cells decreased in size, rearranged their Actin cytoskeleton and retained a partly mesenchymal phenotype. Epithelial characteristics such as adherens junctions and tight junctions were not established before D12 when the pluripotency markers TRA-1-60, Nanog, UTF1 and DPPA2 were upregulated, thus suggesting a synchronized acquisition of epithelial and pluripotent traits. We speculated whether this could be due to the fibroblast culture conditions during the first six days of our reprogramming protocol, which could potentially delay MET. However no colonies emerged when we cultured our reprogramming cells in stem cell conditions from day 1 post-electroporation. Thus, we propose that the discrepancy in the timing of MET may be a matter of species-related differences in reprogramming dynamics, given that most of aforementioned studies were performed with MEFs. This is supported by three other studies of human fibroblasts undergoing reprogramming to iPSCs, which reported E-cadherin expression beginning between days 6 and 15 of reprogramming (Onder et al., 2012; Subramanyam et al., 2011b) and TRA-1-60 positive hiPSC colonies emerging between days 11 and 15 of reprogramming (Takahashi et al., 2014).

It was recently shown that promoting a brief mesenchymal phase prior to the MET could enhance the formation of both mouse and human iPSC colonies (Liu et al., 2013; Di et

al., 2014). The hypothesis that mesenchymal cells must undergo an EMT-like reinforcement before turning their fate towards becoming a pluripotent epithelium correlates with our preliminary observations of Beta-catenin accumulating in the nucleus during the Initiation phase of reprogramming. Nuclear translocation of Beta-catenin is a hallmark of Canonical Wnt signaling and EMT, whereas recruitment of Beta-catenin to the plasma membrane indicates the formation of epithelial adherens junctions and MET (Zeisberg and Neilson, 2009; Kam and Quaranta, 2009). Thus, the presumed movement of Beta-catenin from the cytoplasm to the nucleus between days 0 and 6 in our reprogramming experiments, and from the nucleus to the plasma membrane between days 6 and 12, supports the sequential EMT–MET dynamics reported in Liu et al. (2013).

Conclusion

Here, we provide the first combined ultrastructural, immunocytochemical and gene expression analysis of human fibroblasts at various stages of episomal iPSC reprogramming, as well as the first real-time live cell visualization of MET during reprogramming. Our results indicate that the MET occurs approximately 6–12 days after electroporation in synchrony with the upregulation of pluripotency markers, and resembles a reversal of the EMT which takes place during mammalian gastrulation.

Supplementary data to this article can be found online at <http://dx.doi.org/10.1016/j.scr.2014.11.003>.

Author contribution

M. K. Høffding designed and performed experiments, analyzed data and wrote the paper.

P. Hyttel contributed to design of study, data analysis and interpretation as well as manuscript revision.

Acknowledgments

The research leading to these results has received funding from the People Programme (Marie Curie Actions) of the European Union's Seventh Framework Programme FP7/2007-2013/under REA grant agreement n° PIAPP-GA-2012-324451. Additionally, this work was partly supported by the Danish National Advanced Technology Foundation grant number 047-2011-1, and by the U.S. Department of Agriculture award 2011-67015-30688. Imaging data were collected at the Center for Advanced Bioimaging (CAB) Denmark, University of Copenhagen. We thank PhD Mikkel Aabech Rasmussen and Professor Alexander Schulz for their scientific advice and discussion, and Dr. Christine Gilles for providing the Vimentin promoter-GFP reporter construct. Finally, we would like to express our gratitude to Professor Kjeld Møllgård and PhD Christian Beltoft Brøchner for proof reading of the manuscript.

References

Takahashi, K., Yamanaka, S., 2006. Induction of pluripotent stem cells from mouse embryonic and adult fibroblast cultures by defined factors. *Cell* 126, 663–676.

- Li, R., Liang, J., Ni, S., Zhou, T., Qing, X., Li, H., He, W., Chen, J., Li, F., Zhuang, Q., Qin, B., Xu, J., Li, W., Yang, J., Gan, Y., Qin, D., Feng, S., Song, H., Yang, D., Zhang, B., Zeng, L., Lai, L., Esteban, M.A., Pei, D., 2010. A mesenchymal-to-epithelial transition initiates and is required for the nuclear reprogramming of mouse fibroblasts. *Cell Stem Cell* 7, 51–63.
- Samavarchi-Tehrani, P., Golipour, A., David, L., Sung, H.K., Beyer, T.A., Datti, A., Woltjen, K., Nagy, A., Wrana, J.L., 2010. Functional genomics reveals a BMP-driven mesenchymal-to-epithelial transition in the initiation of somatic cell reprogramming. *Cell Stem Cell* 7, 64–77.
- Kalluri, R., Weinberg, R.A., 2009. The basics of epithelial–mesenchymal transition. *J. Clin. Invest.* 119, 1420–1428.
- Ferrer-Vaquer, A., Viotti, M., Hadjantonakis, A.K., 2010. Transitions between epithelial and mesenchymal states and the morphogenesis of the early mouse embryo. *Cell Adhes. Migr.* 4, 447–457.
- Zeisberg, M., Neilson, E.G., 2009. Biomarkers for epithelial–mesenchymal transitions. *J. Clin. Invest.* 119, 1429–1437.
- Liao, B., Bao, X., Liu, L., Feng, S., Zovoilis, A., Liu, W., Xue, Y., Cai, J., Guo, X., Qin, B., Zhang, R., Wu, J., Lai, L., Teng, M., Niu, L., Zhang, B., Esteban, M.A., Pei, D., 2011. MicroRNA cluster 302–367 enhances somatic cell reprogramming by accelerating a mesenchymal-to-epithelial transition. *J. Biol. Chem.* 286, 17359–17364.
- Subramanyam, D., Lamouille, S., Judson, R.L., Liu, J.Y., Bucay, N., Derynck, R., Belloch, R., 2011. Multiple targets of miR-302 and miR-372 promote reprogramming of human fibroblasts to induced pluripotent stem cells. *Nat. Biotechnol.* 29, 443–448.
- Shu, X., Pei, D., 2014. The function and regulation of mesenchymal-to-epithelial transition in somatic cell reprogramming. *Curr. Opin. Genet. Dev.* 28C, 32–37.
- Lee, M.R., Prasain, N., Chae, H.D., Kim, Y.J., Mantel, C., Yoder, M.C., Broxmeyer, H.E., 2013. Epigenetic regulation of NANOG by miR-302 cluster-MBD2 completes induced pluripotent stem cell reprogramming. *Stem Cells* 31, 666–681.
- Wang, G., Guo, X., Hong, W., Liu, Q., Wei, T., Lu, C., Gao, L., Ye, D., Zhou, Y., Chen, J., Wang, J., Wu, M., Liu, H., Kang, J., 2013. Critical regulation of miR-200/ZEB2 pathway in Oct4/Sox2-induced mesenchymal-to-epithelial transition and induced pluripotent stem cell generation. *Proc. Natl. Acad. Sci. U. S. A.* 110, 2858–2863.
- Li, Z., Yang, C.S., Nakashima, K., Rana, T.M., 2011. Small RNA-mediated regulation of iPS cell generation. *EMBO J.* 30, 823–834.
- Chen, M., Zhang, H., Wu, J., Xu, L., Xu, D., Sun, J., He, Y., Zhou, X., Wang, Z., Wu, L., Xu, S., Wang, J., Jiang, S., Zhou, X., Hoffman, A.R., Hu, X., Hu, J., Li, T., 2012. Promotion of the induction of cell pluripotency through metabolic remodeling by thyroid hormone triiodothyronine-activated PI3K/AKT signal pathway. *Biomaterials* 33, 5514–5523.
- Takahashi, K., Tanabe, K., Ohnuki, M., Narita, M., Sasaki, A., Yamamoto, M., Nakamura, M., Sutou, K., Osafune, K., Yamanaka, S., 2014. Induction of pluripotency in human somatic cells via a transient state resembling primitive streak-like mesoderm. *Nat. Commun.* 5, 3678.
- Sakurai, K., Talukdar, I., Patil, V.S., Dang, J., Li, Z., Chang, K.Y., Lu, C.C., Delorme-Walker, V., Dermardirossian, C., Anderson, K., Hanein, D., Yang, C.S., Wu, D., Liu, Y., Rana, T.M., 2014. Kinome-wide functional analysis highlights the role of cytoskeletal remodeling in somatic cell reprogramming. *Cell Stem Cell* 14, 523–534.
- Hu, X., Zhang, L., Mao, S.Q., Li, Z., Chen, J., Zhang, R.R., Wu, H.P., Gao, J., Guo, F., Liu, W., Xu, G.F., Dai, H.Q., Shi, Y.G., Li, X., Hu, B., Tang, F., Pei, D., Xu, G.L., 2014. Tet and TDG mediate DNA demethylation essential for mesenchymal-to-epithelial transition in somatic cell reprogramming. *Cell Stem Cell* 14, 1–11.
- Onder, T.T., Kara, N., Cherry, A., Sinha, A.U., Zhu, N., Bernt, K.M., Cahan, P., Marcarci, B.O., Unternaehrer, J., Gupta, P.B., Lander, E.S., Armstrong, S.A., Daley, G.Q., 2012. Chromatin-modifying enzymes as modulators of reprogramming. *Nature* 483, 598–602.
- Liang, G., He, J., Zhang, Y., 2012. Kdm2b promotes induced pluripotent stem cell generation by facilitating gene activation early in reprogramming. *Nat. Cell Biol.* 14, 457–466.
- Okita, K., Matsumura, Y., Sato, Y., Okada, A., Morizane, A., Okamoto, S., Hong, H., Nakagawa, M., Tanabe, K., Tezuka, K., Shibata, T., Kunisada, T., Takahashi, M., Takahashi, J., Saji, H., Yamanaka, S., 2011. A more efficient method to generate integration-free human iPS cells. *Nat. Methods* 8, 409–412.
- Niwa, H., Yamamura, K., Miyazaki, J., 1991. Efficient selection for high-expression transfectants with a novel eukaryotic vector. *Gene* 108, 193–199.
- Bindels, S., Mestdagt, M., Vandewalle, C., Jacobs, N., Volders, L., Noel, A., van RF, Berx G., Foidart, J.M., Gilles, C., 2006. Regulation of vimentin by SIP1 in human epithelial breast tumor cells. *Oncogene* 25, 4975–4985.
- Gilles, C., Polette, M., Zahm, J.M., Tournier, J.M., Volders, L., Foidart, J.M., Birembaut, P., 1999. Vimentin contributes to human mammary epithelial cell migration. *J. Cell Sci.* 112 (Pt 24), 4615–4625.
- Gilles, C., Polette, M., Mestdagt, M., Nawrocki-Raby, B., Ruggeri, P., Birembaut, P., Foidart, J.M., 2003. Transactivation of vimentin by beta-catenin in human breast cancer cells. *Cancer Res.* 63, 2658–2664.
- Hall, V.J., Jacobsen, J.V., Rasmussen, M.A., Hyttel, P., 2010. Ultrastructural and molecular distinctions between the porcine inner cell mass and epiblast reveal unique pluripotent cell states. *Dev. Dyn.* 239, 2911–2920.
- Wolf, X.A., Serup, P., Hyttel, P., 2011. Three-dimensional localisation of NANOG, OCT4, and E-CADHERIN in porcine pre- and peri-implantation embryos. *Dev. Dyn.* 240, 204–210.
- Gasser, R.F., 1975. The second week of life: bilaminar and early trilaminar period. *Atlas of Human Embryos. The Endowment For Human Development, Inc.*, pp. 7–13.
- Brosh, R., Assia-Alroy, Y., Molchadsky, A., Bornstein, C., Dekel, E., Madar, S., Shetzer, Y., Rivlin, N., Goldfinger, N., Sarig, R., Rotter, V., 2013. p53 counteracts reprogramming by inhibiting mesenchymal-to-epithelial transition. *Cell Death Differ.* 20, 312–320.
- Rasmussen, M.A., Holst, B., Tumer, Z., Johnsen, M.G., Zhou, S., Stummann, T.C., Hyttel, P., Clausen, C., 2014. Transient p53 suppression increases reprogramming of human fibroblasts without affecting apoptosis and DNA damage. *Stem Cell Rep.* 3, 404–413.
- Pera, M.F., Trounson, A.O., 2004. Human embryonic stem cells: prospects for development. *Development* 131, 5515–5525.
- Hertig, A.T., Rock, J., 1945. Two human ova of the pre-villous stage, having a development age of about eight and nine days respectively. *Contrib Embryol.* 33. Carnegie, Institution of Washington, pp. 169–186
- Hertig, A.T., Rock, J., 1949a. Two human ova of the pre-villous stage, having a development age of about seven and nine days. *Contrib Embryol.* 31. Carnegie Institution of Washington, pp. 65–84
- Hertig, A.T., Rock, J., 1949b. Two human ova of the pre-villous stage, having an ovulation age of about eleven and twelve days respectively. *Contrib Embryol.* 29. Carnegie Institution of Washington, pp. 127–156.
- David, L., Polo, J.M., 2014. Phases of reprogramming. *Stem Cell Res.* 12, 754–761.
- Mikkelsen, T.S., Hanna, J., Zhang, X., Ku, M., Wernig, M., Schorderet, P., Bernstein, B.E., Jaenisch, R., Lander, E.S., Meissner, A., 2008.

- Dissecting direct reprogramming through integrative genomic analysis. *Nature* 454, 49–55.
- Sridharan, R., Tchiew, J., Mason, M.J., Yachechko, R., Kuoy, E., Horvath, S., Zhou, Q., Plath, K., 2009. Role of the murine reprogramming factors in the induction of pluripotency. *Cell* 136, 364–377.
- Stadtfeld, M., Maherali, N., Breault, D.T., Hochedlinger, K., 2008. Defining molecular cornerstones during fibroblast to iPS cell reprogramming in mouse. *Cell Stem Cell* 2, 230–240.
- Polo, J.M., Anderssen, E., Walsh, R.M., Schwarz, B.A., Nefzger, C.M., Lim, S.M., Borkent, M., Apostolou, E., Alaei, S., Cloutier, J., Bar-Nur, O., Cheloufi, S., Stadtfeld, M., Figueroa, M.E., Robinton, D., Natesan, S., Melnick, A., Zhu, J., Ramaswamy, S., Hochedlinger, K., 2012. A molecular roadmap of reprogramming somatic cells into iPS cells. *Cell* 151, 1617–1632.
- Hansson, J., Rafiee, M.R., Reiland, S., Polo, J.M., Gehring, J., Okawa, S., Huber, W., Hochedlinger, K., Krijgsveld, J., 2012. Highly coordinated proteome dynamics during reprogramming of somatic cells to pluripotency. *Cell Rep.* 2, 1579–1592.
- Brambrink, T., Foreman, R., Welstead, G.G., Lengner, C.J., Wernig, M., Suh, H., Jaenisch, R., 2008. Sequential expression of pluripotency markers during direct reprogramming of mouse somatic cells. *Cell Stem Cell* 2, 151–159.
- Tanabe, K., Nakamura, M., Narita, M., Takahashi, K., Yamanaka, S., 2013. Maturation, not initiation, is the major roadblock during reprogramming toward pluripotency from human fibroblasts. *Proc. Natl. Acad. Sci. U. S. A.* 110, 12172–12179.
- Liu, X., Sun, H., Qi, J., Wang, L., He, S., Liu, J., Feng, C., Chen, C., Li, W., Guo, Y., Qin, D., Pan, G., Chen, J., Pei, D., Zheng, H., 2013. Sequential introduction of reprogramming factors reveals a time-sensitive requirement for individual factors and a sequential EMT–MET mechanism for optimal reprogramming. *Nat. Cell Biol.* 15, 829–838.
- Di, S.B., Sardina, J.L., van OC, Collombet S., Kallin, E.M., Vicent, G.P., Lu, J., Thieffry, D., Beato, M., Graf, T., 2014. C/EBPalpha poises B cells for rapid reprogramming into induced pluripotent stem cells. *Nature* 506, 235–239.
- Kam, Y., Quaranta, V., 2009. Cadherin-bound beta-catenin feeds into the Wnt pathway upon adherens junctions dissociation: evidence for an intersection between beta-catenin pools. *PLoS One* 4, e4580.
- Reynold, E.S., 1963. The use of lead citrate at high pH as an electron-opaque stain in electron microscopy. *J. Cell Biol.* 208–212 PMID: 13986422.